

DETC2017-67386

**COST MINIMIZATION IN METAL ADDITIVE MANUFACTURING USING
CONCURRENT STRUCTURE AND PROCESS OPTIMIZATION**

Runze Huang

Department of Mechanical Engineering
Carnegie Mellon University, Pittsburgh, PA, USA

Erva Ulu

Department of Mechanical Engineering
Carnegie Mellon University, Pittsburgh, PA, USA

Levent Burak Kara

Department of Mechanical Engineering
Carnegie Mellon University, Pittsburgh, PA, USA

Kate S. Whitefoot*

Department of Mechanical Engineering,
Department of Engineering and Public Policy
Carnegie Mellon University, Pittsburgh, PA, USA

ABSTRACT

Metals-additive manufacturing (MAM) is enabling unprecedented design freedom and the ability to produce significantly lighter weight parts with the same performance, offering the possibility of significant environmental and economic benefits in many different industries. However, the total production costs of MAM will need to be reduced substantially before it will be widely adopted across the manufacturing sector. Current topology optimization approaches focus on reducing total material volume as a means of reducing material costs, but they do not account for other production costs that are influenced by a part's structure such as machine time and scrap. Moreover, concurrently optimizing MAM process variables with a part's structure has the potential to further reduce production costs. This paper demonstrates an approach to use process-based cost modeling in MAM topology optimization to minimize total production costs, including material, labor, energy, and machine costs, using cost estimates from actual MAM operations. The approach is demonstrated in a simple case study of a Ti64 cantilever produced with electron beam melting (EBM). Results of a concurrent optimization of the part structure and EBM process variables are compared to an optimization of the part structure alone. The results show that, once process variables are considered, it is more cost effective to include more material in the part through a combination of (1) building additional thin trusses with a faster laser speed and (2) increasing the thickness of other truss members and decreasing laser velocity to create larger melt pools that reduce the number of passes required, thereby

reducing build time. Concurrent optimization of the part's structure and MAM process parameters leads to 7% lower estimated total production costs and approximately 50% faster build time than optimizing the part's structure alone.

1. INTRODUCTION

Metals-additive manufacturing (MAM) has the potential to offer unprecedented design freedom by allowing complex geometries to be created that are impossible or cost prohibitive to produce through traditional manufacturing methods [1]. It is also enabling the production of significantly lighter weight parts with the same performance, offering the possibility of significant environmental and economic benefits in many industries, including aerospace, medical, and energy [1-3]. However, relatively high production costs of MAM are preventing widespread adoption across many manufacturing sectors [1, 4]. Studies have demonstrated that optimizing the structural design of MAM parts can help decrease material usage, and therefore material costs, while maintaining part performance [5-7]. The classic topology optimization formulation minimizes compliance or stress subject to a constraint on the total volume [8-11], representing a proxy for material costs [12-16]. However, a part's topology also influences production costs through means other than the costs associated with the material contained in the final part. For example, scrap and energy costs depend on where exactly material in the machine build envelope is added to a part and where it is not [4]. Furthermore, MAM process variables, such as laser power and speed, influence production costs associated with machine time and energy as well as material properties

*Corresponding author: kwhitefoot@cmu.edu

[17]. Concurrent optimization of MAM process variables and a part's topology therefore has the potential to further reduce production costs. While the potential to optimize AM process parameters and part topology has been discussed in literature [18, 19] and empirical case studies have been presented to optimize process parameters given a fixed topology [20-25], no previous literature has concurrently optimized a part's topology as well as process variables. Moreover, no existing methodologies have been developed to minimize total production costs in a topology optimization, which, as we discuss, can lead to significantly different part designs than the standard topology optimization formulation.

In this paper, we demonstrate a production cost minimization approach for MAM that concurrently optimizes the part structure and process variables, including laser power and velocity (Figure 1). The approach is developed by integrating efficient topology optimization, process-based cost modeling (PBCM), and MAM process/solidification mapping between process variables and microstructure. The main focus of the paper is to present the methodology and demonstrate that accounting for the influence of both structural design and MAM process parameters on total production costs can lead to different design topology solutions that have more material usage but lower total production costs compared to solely optimizing the structure.

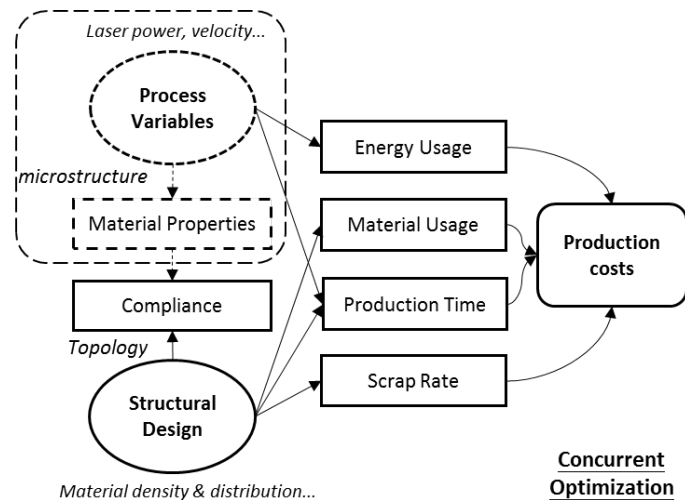


Figure 1. Cost minimization framework. The dashed lines contain the elements included in the concurrent optimization but not the optimization of structural design alone.

2. LITERATURE REVIEW

We draw on three different methods to develop the methodology presented in this paper: topology optimization, process-based modeling, and process mapping for MAM. This section describes these methods and reviews past work relevant to AM.

2.1 DESIGN AND TOPOLOGY OPTIMIZATION FOR ADDITIVE MANUFACTURING

Due to the unique capabilities of additive manufacturing (AM), new methods and tools are needed to improve design for AM (DFAM) to maximize product performance [12]. One class of methods ripe for adaptation for DFAM is topology optimization—a powerful technique in structural design that optimizes the shape and material connectivity of a domain through the use of finite element methods together with various optimization techniques [8, 26]. Topology optimization has been extensively applied for designing AM parts [13, 14, 19]. Recent adaptations of topology optimization for DFAM include considering the constraints of support structures [15], internal patterns [27], as well as applications in design of cellular structures [28], heat sinks [16], and tissue scaffolds [7]. However, these existing topology optimization approaches have not yet considered the influence of AM structural design on total production costs or the significance of considering process variables in reducing these costs. Density-based topology optimization approaches are one of the available methods in the literature [11, 29, 30]. These methods approach the design problem in a way that the structure is defined by optimizing the material distribution in the domain. Since each finite element within the design domain is defined as a design variable, these methods provide extensive flexibility in design allowing the resulting geometry to be highly complex. The objectives of most existing AM topology optimization approaches focus on minimizing compliance, or maximizing stress safety factors of the structure with respect to the density of elements within the part [31], but they do not consider the production cost of AM.

2.2 COSTS OF AM PROCESSES AND PROCESS-BASED COST MODELING

A variety of studies have been conducted to identify the main factors that influence AM production costs. Thomas et al. performed a literature review of economic studies and cost models of polymeric and metallic AM processes [4]. Hopkinson and Dickens analyzed the costs of polymeric AM and compared them with the cost of injection molded parts [32]. Ruffo et al. developed an AM cost model that estimated different cost drivers for powder based selective laser sintering processes [33]. Other AM cost models and prediction tools have been developed by Lindemann et al. [34, 35], Baumers et al. [17, 36], and Rickenbacher et al. [37]. In these studies, material usage, build time, laser power, scan speed, hatch spacing, and production volume have all been found to significantly influence production costs.

Despite this work identifying the major factors that drive AM costs, studies that incorporate cost assessment to support DFAM are limited. Yim and Rosen developed an AM selection tool based on cost estimation [38]. Yao et al developed a cost-driven design methodology for AM platforms in product families [39]. These studies guide the selection of different AM techniques based on the lower-cost methods, but none of them offer an optimization approach to select AM designs that minimize production costs.

Process-based cost modeling (PBCM) was developed for assessing the economic performance of new technologies under changing design specifications and manufacturing operations [40]. The method is based on simulating production process parameters (e.g., cycle times, yields, scrap rates) depending on the physical design of a part (e.g., geometry, material selection) and the process design (e.g., manufacturing steps and equipment) to highlight the implications of changing design variables and operating conditions on production costs. PBCM has been applied to analyze the production costs of new technologies or designs such as composite automobile body production [41], electronic semiconductor chip design [42] and optoelectronic transceiver assembly [43]. Laureijs et al. demonstrated the potential of using PBCM for MAM by analyzing the cost competitiveness of an MAM engine bracket compared to a comparable design produced by forging [44]. Because PBCM is focused on analyzing the production costs associated with alternative design solutions, we chose PBCM as the methodology to account for production costs in a MAM topology optimization in this study.

2.3 PROCESS/SOLIDIFICATION MAPPING FOR ADDITIVE MANUFACTURING

The process variables of MAM machines not only influence the production costs, but also determine the process characteristics (e.g., melt pool dimensions) [45], material microstructure (e.g., grain size, porosity) [46], and material properties (e.g., strength, fatigue) [47, 48]. Process and solidification mapping were developed by Gockel et al. [45, 49], Beuth et al. [50, 51], Montgomery et al. [52], and Seifi et al. [47] to predict and control the desired MAM process outcomes through melt pool and microstructure forming through production. The absorbed laser power and the laser moving speed determines the local cooling rate of the material, which directly influences the melt pool geometry, the grain morphology and grain size. For Ti64, higher laser power or lower laser speed leads to larger melt pool area and larger grain size, which reduces the yield strength of the material [53-55]. Studies have found that the grain size of Ti64 in MAM is approximately linear to the melt pool width [53], and the yield strength of the metal is approximately linear to the inverse square root of grain size by the Hall-Petch strengthening relationship [56]. We use the results of these studies to represent the relationships between MAM process variables and material properties in order to minimize production costs subject to a part's performance constraints.

3. METHOD

3.1 MAM PRODUCTION COST MODEL

In order to minimize production cost of MAM processes, a general mathematical representation of MAM production cost is developed based on the typical PBCM approach. Estimates for each of the constituent factor costs in the model are taken from data collected from MAM operations in fourteen companies according to Laureijs et al. [44].

The production costs that are influenced by structural and/or process variables are broken into two categories: those that contribute to material-based costs and those that contribute to time-based costs [4]. The material-based costs include the material required for printing the design of the part, and material scrap that is lost during powder recovery and recycling. The time-based cost includes the machine cost amortized by the production time necessary to produce the required throughput yield, the energy cost, and other costs depending on the production time such as labor required to run the machine. Since the goal of the paper is to demonstrate the design difference driven by incorporating cost minimization, structural optimization, and process variables, other production costs that are not affected by structural or process variables, such as management overhead costs, are not included. The cost formulation is as follows:

$$C(V_{part}, t, P) = A_1 V_{part} + A_2 t + A_3 \int_{t_0}^t P dt + A_4 \quad (1)$$

where V is the volume of the part, P is the power required for printing, and t is the total production time required for the part. A_i are coefficients that characterize MAM machines and factor input costs such as labor and electricity (Table 1). The detailed derivation is documented in ANNEX A.

Table 1. Formulation of the constituent factor costs

	Coefficient description	Unit	Formulation
A_1	Material cost	\$/cm ³	$c_m \rho (1 - \eta)$
A_2	Manufacturing cost	\$/min	$\frac{c_{invest} + c_{maintain} * L}{L * H} + c_{labor}$
A_3	Energy cost	\$/Wh	c_{elec}
A_4	Scrap and idle electricity cost	\$	$c_m \rho \eta V_{envelope} + c_{elec} P_0 t$

The constituent factor costs applied in this cost model—material price, c_m , machine price, c_{invest} , maintenance cost, $c_{maintain}$, labor cost, c_{labor} , energy cost, c_{elec} , and scrap rate, η —are based on the PBCM data developed by Laureijs et al. [44]. The data were based on the EBM process with Ti64 produced in the United States with an annual production volume of 13,500 or greater.

3.2 PROCESS MAPPING

Total required production time is one major driver of production costs in the formulation shown in equation 1. The time is composed of the setup time, laser sintering time, powder delivery time, and cooling time [17]. For simplicity, we assume that the setup time and cooling time are the same for any print jobs since the geometry has limited influence on these time factors [17]. Additionally, we assume that powder delivery time is constant if the layer thickness and the z-axis height of the part is the same. The production time can therefore be represented as:

$$t = t_{build} + t_0 \quad (2)$$

where t_0 is a constant, and t_{build} depends on the design and process parameters.

As discussed in Section 2.3, process-solidification maps have been developed for different MAM processes and can be applied in controlling or predicting melt pool geometry with certain process parameters (e.g., absorbed power, αP , and velocity, v) [45]. The approximate analytical descriptions of the process-solidification map can be derived from the Rosenthal equation [57, 58]. Following this approach, the melt pool area, A , the melt pool depth, d , and the melt pool width, W , can be estimated as:

$$A = \frac{a_1 \alpha P + a_2}{v} \quad (3)$$

$$d = 0.5W = \sqrt{\frac{2A}{\pi}} = \sqrt{\frac{2(a_1 \alpha P + a_2)}{\pi v}} \quad (4)$$

where a_1 and a_2 are constant factors that relate to the material. Assuming half overlap between melt pool in the building process to ensure full melting, t_{build} in every layer can be estimated as:

$$t_{build} = \int \frac{1}{vd} d\Gamma = \int \sqrt{\frac{\pi}{2v(a_1 \alpha P + a_2)}} d\Gamma \quad (5)$$

where Γ is the full building envelope area in every layer. As a result, the production cost can be formulated as a function of part volume, laser power, and laser velocity.

In addition to the influence they have on production costs, melt pool dimension directly influence the microstructure of a material and the mechanical properties of a part. Studies have found that the grain size of Ti64 in MAM is approximately linear to the melt pool width [53], and the yield strength of the metal is approximately linear to the inverse square root of grain size by the Hall-Petch strengthening relationship [56]. Based on the process mapping and Hall-Petch strengthening relationship [53-56], the yield strength can be formulated as:

$$\sigma_y = \frac{b_1}{\sqrt{d_{grain}}} + a_4 = a_3 \left[\frac{2(a_1 \alpha P + a_2)}{\pi v} \right]^{-\frac{1}{4}} + a_4 \quad (6)$$

The parameters b_1 and a_4 are coefficients estimated based on Hall-Petch strengthening relationship, and a_3 is a parameter proportional to b_1 that is experimentally determined for the specific material.

As displayed in Figure 2, the yield strength of the MAM material can be approximately estimated from the process parameters (absorbed power, αP , and velocity, v) through melt pool dimension and grain size estimated by the process mapping. Importantly, because laser speed and power affect the melt pool size, they also influence the number of passes of the laser that are required to build the same part. Figure 3 illustrates how laser speed affects the number of passes required of the laser path under the same laser power.

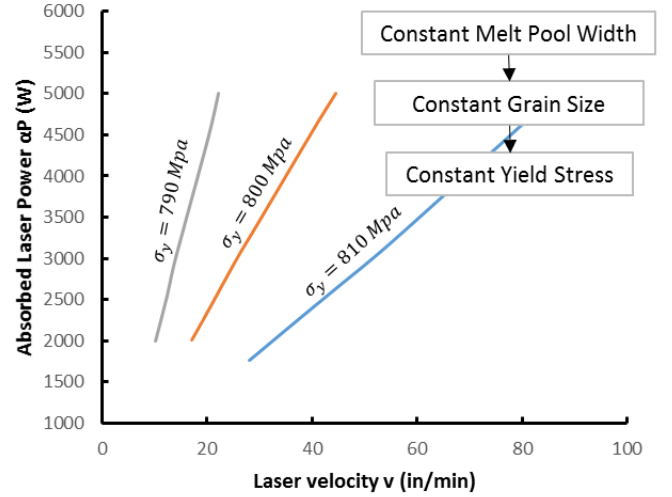


Figure 2. Demonstration of process mapping of MAM processes for Ti64. The process variables at the same line leads to the same yield stress.

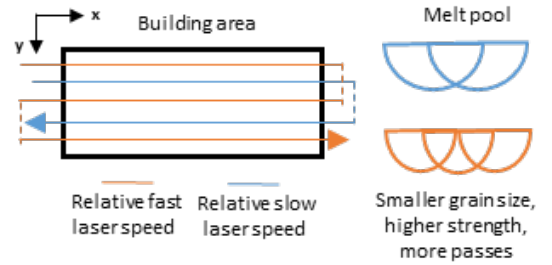


Figure 3. Illustration of the influence of laser speed, melt pool size, and the number of passes to cover a building area.

3.3 TOPOLOGY AND PROCESS OPTIMIZATION

A density-based approach and a modified SIMP method are applied for topology optimization. Heuristic relationships are applied between element density, x_i , element laser power, P_i , element laser velocity, v_i , element Young's modulus, E_i , and yield strength, Y_i , given by:

$$E_i(x_i) = E_{min} + x_i^p (E_0 - E_{min}) \quad (7)$$

$$Y_i(x_i, P_i, v_i) = Y_{min} + x_i^p (\sigma_y - Y_{min}) \\ = Y_{min} + x_i^p \left\{ a_3 \left[\frac{2(a_1 \alpha P_i + a_2)}{\pi v_i} \right]^{-\frac{1}{4}} + a_4 - Y_{min} \right\} \quad (8)$$

where E_{min} and Y_{min} are the elastic modulus and yield strength of the void material, respectively, and p is the penalty factor. E_0 is the Young's modulus of the material. In order to avoid numerical difficulties such as the checkerboard issue [59], sensitivity filters are applied to the element density, laser power, and velocity based on [60]:

$$\tilde{x}_i = \frac{\sum_{j \in N_i} H_{ij} V_j x_j}{\sum_{j \in N_i} H_{ij} V_j} \quad (9)$$

$$N_i = \{j: \text{dist}(i, j) \leq R\} \quad (10)$$

$$H_{ij} = R - \text{dist}(i, j) \quad (11)$$

where N_i is the neighborhood of element x_i with volume V_j , H_{ij} is a weight factor, and \tilde{x}_i represents the updated density with sensitivity filters. With discretization using hexagonal elements and equation (5), the time estimation and production cost function can be written as:

$$t_{build}(v_i, P_i) = \sum_i N_i t_{pass_i} = \sum_i \frac{l_{xi} l_{yi}}{v_i d_i} \quad (12)$$

$$= \sum_i l_{xi} l_{yi} \sqrt{\frac{\pi}{2v_i(a_1 \alpha P_i + a_2)}}$$

$$C(x_i, P_i, v_i) = A_1 l_x l_y l_z \sum_i x_i \quad (13)$$

$$+ A_2 l_x l_y \sqrt{\pi} \sum_i [2v_i(a_1 \alpha P_i + a_2)]^{-\frac{1}{2}}$$

$$+ A_3 l_x l_y \sqrt{\pi} \sum_i P_i [2v_i(a_1 \alpha P_i + a_2)]^{-\frac{1}{2}} + A_4 + A_2 t_0$$

where N_i is the number of passes, t_{pass_i} is the time for each pass of the laser, and l_x , l_y , and l_z are the length of the element at x, y, and z directions, respectively.

The compliance of the structure is applied in the topology optimization as:

$$c_o(\tilde{x}_i) = E_i(\tilde{x}_i) \mathbf{u}_i^T \mathbf{k}_0 \mathbf{u}_i \quad (14)$$

where \mathbf{k}_0 is the element stiffness matrix for an element with unit Young's modulus and \mathbf{C}_0 is the unit constitutive matrix. The maximum of the compliance allowed within the structure is given by:

$$c_{o_{max}}(\tilde{x}, \tilde{P}, \tilde{v}) = E_i(\tilde{x}_i) k^2 \mathbf{Y}_i^T(\tilde{x}, \tilde{P}, \tilde{v}) (\mathbf{C}_0^{-1})^T \mathbf{Y}_i(\tilde{x}, \tilde{P}, \tilde{v}) \quad (15)$$

where \mathbf{Y}_i is the element yield strength matrix and k is the safety factor. The derivation can be found in the ANNEX A

The mathematical formulation of the optimization problem is as follows:

$$\min_{x, P, v} C(\tilde{x}, \tilde{P}, \tilde{v})$$

$$\text{subject to: } \mathbf{h}_1(\tilde{x}) = \mathbf{K}\mathbf{U} - \mathbf{F} = \mathbf{0}$$

$$g_1(\tilde{x}) = V(\tilde{x})/V_0 - f \leq 0$$

$$g_2(\tilde{x}, \tilde{P}, \tilde{v}) = c_o(\tilde{x}_i) - c_{o_{max}}(\tilde{x}, \tilde{P}, \tilde{v}) \leq 0$$

$$\text{And } \chi = \{0 \leq \mathbf{x} \leq 1, 0 \leq \mathbf{P} \leq P_0, 0 \leq \mathbf{v} \leq v_0\}$$

where C is the production cost, c_o is the compliance, \mathbf{U} and \mathbf{F} are the global displacement and force vectors, \mathbf{K} is the global stiffness matrix, and \mathbf{u}_i is the element displacement vector. \mathbf{P} , \mathbf{v} , and \mathbf{x} are the product and process design variables, specifically laser power, laser velocity, and elemental

density, respectively. N is the number of elements used to discretize the design domain, $V(\tilde{x})$ and V_0 are the material volume and design domain volume, and f is the prescribed volume fraction.

3.4 NUMERICAL IMPLEMENTATION AND TEST CASE

A basic cantilevered beam (Figure 4) was used as the case study to demonstrate the developed methodology and the design improvement enabled by the concurrent optimization. A distributed vertical load is applied downwards on the lower free edge, while the prismatic design domain is fully constrained at the other end. Considering data availability, the MAM process is assumed as EBM, and the material is assumed as Ti64 alloy. Table 2 summarizes the basic parameters that are applied in the optimization algorithm.

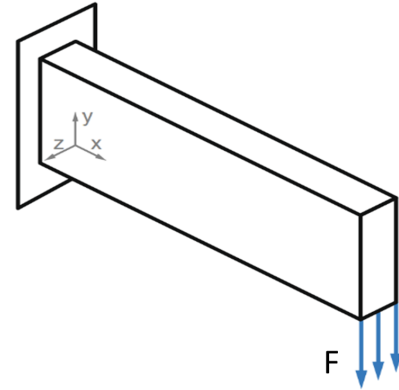


Figure 4. Loading conditions used in the case study demonstration.

Table 2. Input parameters to the algorithm

Parameter	Description	Unit	Value
c_m	Material unit cost	\$/kg	250
ρ	Density	g/cm ³	4.5
η	Scrap rate	%	0.1
c_{invest}	Machine investment cost	1000\$	1100
$c_{maintain}$	Maintenance cost	1000\$	50
L	Life time	year	7
H	Annual working time	h/year	7000
c_{labor}	Labor unit cost	\$/h	26
c_{elec}	Electricity unit cost	\$/kwh	0.03
a_1	P-V coefficient	in ³ /W min	0.000302
α	absorb ratio	-	0.9
a_2	P-V coefficient	in ³ /min	-0.08941
a_3	Property coefficient	Mpa (μm) ^{-0.5}	519.7
a_4	Property coefficient	Mpa	772.2
E_{min}	Young's modulus of void material	Gpa	10-9

E_0	Young's modulus	Gpa	100
Y_{min}	Yield strength of void material	Mpa	10-6
l_x, l_y, l_z	element length	cm	1
P_0	Initial value for power	W	2000
v_0	Initial value for velocity	in/min	40
F	Applied force	kN	10000
p	Penalty factor	-	3
n_x	Number of element in the x direction	-	60
n_y	Number of element in the y direction	-	20
n_z	Number of element in the z direction	-	1

The optimization is implemented with MATLAB based on the efficient 3D topology optimization code developed by Liu and Tovar [61]. The solution is determined using trust-region sequential quadratic programming. Derivatives and Hessians of the objective and constraint functions were analytically derived and applied in the algorithms to reduce computing efforts.

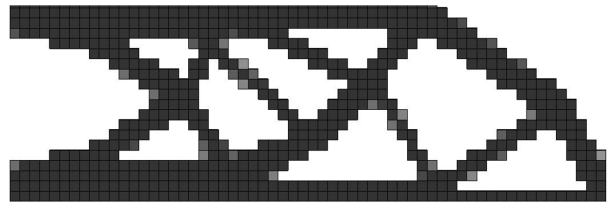
4. RESULTS AND DISCUSSION

Figure 5 shows the comparison of the optimization of the 3D cantilever beam using two different formulations. Figure 3(a) shows the design solution that minimizes total production costs with respect to the structure but does not consider process variables, i.e. P and v are set as the initial values. Figure 3(b) shows the design solution that minimizes total production costs using a concurrent optimization of the structure and process variables. By optimizing P and v for each element, the concurrent solution It contains additional truss structures that have thinner truss members with high yield strength that are produced with relatively fast laser speed, while also containing thicker trusses in parts of the top and bottom members that are produced with larger laser power and lower laser speed to achieve faster build rate with fewer passes than the previous design. The difference between the designs highlights that considering process parameters in addition to structure can lead to unique topology solutions for MAM production. The comparison shows an advantage of applying less material in parts of the structure with fine microstructure led by higher laser power and speed, and building more material in other locations with fewer passes by decreasing laser speed, which can only be realized with the concurrent optimization.

Table 3 summarizes the production costs and build time associated with the two different optimization formulations. The concurrent optimization solution shows 7% lower total production costs and 51% faster build time compared to the design of the structural optimization that does not consider process variables. The speed improvement is led by optimizing the structure and process concurrently. In the latter design, the

laser speed and laser power is optimized (ranging from 35-240% of the initial value throughout the part). The slower laser speed leads to larger melt-pool size, requiring fewer passes and thereby reducing build time, but also resulting in larger grain size in the trusses that decreases the yield strength. The reduced yield strength compensated by the additional material and structure applied in the design, which increases material usage. Overall, the total production costs are reduced by considering both structure and process variables. The cost improvement is majorly driven by shorter build time, which leads to savings of 62% machine cost, 51% labor cost, and 48% energy cost. Note that material use increases in this optimization solution, leading to a 31% increase in material cost compared to the design result from solely optimizing the structure, although total production costs are lower with this solution.

a) Cost minimization with only density as changing variables



b) Cost minimization with density, laser power, and laser velocity as changing variables (design (a) shown in blue for reference)

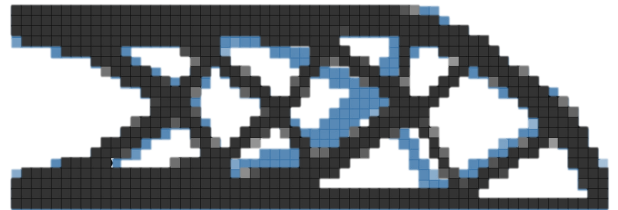


Figure 5. Design comparison between sole optimization of structure (top) and concurrent optimization of structure and process parameters (bottom) in minimizing production costs.

The cost savings are sensitive to the unit material cost and the annual operation hours for MAM machines that assumed in the model. The reduction in total MAM production costs of 7% using the concurrent optimization of structural and process variables found in this study is likely a lower bound for the following reasons: (1) Ti-64 powder is a relatively expensive material (~\$250/kg) so the cost difference is likely to be significantly larger for materials such as steel and aluminum (~\$80/kg); (2) the annual operation hour (~7000 hours/year) for the MAM machine is assumed as the maximum suggested by the machine supplier [62], and the cost improvement could be much larger if annual operating hours are lower. In fact, we find that concurrent optimization leads to a 34% cost reduction if the annual operating hours are assumed to be 2000 hours/year

as suggested by [63]. This cost difference is enough to determine whether AM or conventional manufacturing methods are the least cost option for producing a part [62]. Therefore, the results imply that it may be important to consider process parameters concurrently with a part's structural design when considering whether to manufacture a part with MAM.

Table 3. Cost and time comparison between designs considering different variables

	Solely optimizing structure	Concurrent optimizing structure and process parameters	Improvement from concurrent optimization
Build time	11.6 min	5.7 min	51%
Total cost	\$816.9	\$761.7	7%
Material cost	\$491.2	\$641.3	-31%
Machine cost	\$320.7	\$120.4	62%
Labor cost	\$5.0	\$2.5	51%
Machine energy cost	\$0.01	\$0.005	48%

5. CONCLUSION

This paper demonstrates a cost-minimization approach for MAM topology design that concurrently optimizes the structure and process parameters. The approach demonstrates the capability to reduce total production costs by incorporating a process-based cost model into a topology optimization framework. Additionally, MAM process mapping is combined

REFERENCES

[1] Huang, S., Liu, P., Mokasdar, A., and Hou, L., 2013, "Additive manufacturing and its societal impact: a literature review," *Int J Adv Manuf Technol*, 67(5-8), pp. 1191-1203.

[2] Huang, R., Riddle, M., Graziano, D., Warren, J., Das, S., Nimbalkar, S., Cresko, J., and Masanet, E., 2016, "Energy and emissions saving potential of additive manufacturing: the case of lightweight aircraft components," *Journal of Cleaner Production*, 135, pp. 1559-1570.

[3] Khajavi, S. H., Partanen, J., and Holmström, J., 2014, "Additive manufacturing in the spare parts supply chain," *Computers in Industry*, 65(1), pp. 50-63.

[4] Thomas, D. S., and Gilbert, S. W., 2014, "Costs and Cost Effectiveness of Additive Manufacturing," NIST, National Institute of Standards and Technology, US Department of Commerce.

[5] Tomlin, M., and Meyer, J., 2011, "Topology Optimization of an Additive Layer Manufactured (ALM) Aerospace Part," *Proc. The 7th Altair CAE Technology Conference*, Gaydon, UK, 10th May.

[6] Cheng, L., Zhang, P., Biyikli, E., Bai, J., Robbins, J., Lynch, M. E., Butcher, E. J., and To, A. C., 2016, "Efficient Design Optimization of Variable-Density Cellular Structures for

with topology optimization to compare the results of minimizing costs with respect to structural parameters with a concurrent optimization of structural design and process parameters. The results highlight the potential significance of incorporating process design with topology design in order to reduce production costs and build time.

The approach developed in the paper is merely a proof of concept, and there are several aspects to be improved in future research. The cost model only considers the economic difference of the manufacturing stage and not other life cycle stages, such as cost benefits brought by light-weighting in the use phase. Considering total life cycle costs can cause changes in the design solutions. We plan to develop models that consider full life cycle costing benefits. The approach also did not include optimization of tool path, orientation, packing, production volume, or batch size, which are all influential factors in the production costs. The study also did not consider anisotropy in the optimization, which should be considered for 3D applications. The relationships between process variables and material properties are estimated with first-order approximation, which ideally should be captured through thermal and microstructure simulation to increase accuracy. Additionally, the capability of MAM to achieve unique mesostructure with desired properties can be included in the formulation. In further research, we plan to address these challenges and develop a user-friendly tool for real applications with validation for MAM operations.

Additive Manufacturing: Theory and Experimental Validation," *Rapid Prototyping Journal*.

[7] Wang, X., Xu, S., Zhou, S., Xu, W., Leary, M., Choong, P., Qian, M., Brandt, M., and Xie, Y. M., 2016, "Topological design and additive manufacturing of porous metals for bone scaffolds and orthopaedic implants: a review," *Biomaterials*, 83, pp. 127-141.

[8] Bendsoe, M. P., and Sigmund, O., 2013, *Topology optimization: theory, methods, and applications*, Springer Science & Business Media.

[9] Eschenauer, H. A., and Olhoff, N., 2001, "Topology optimization of continuum structures: a review," *Applied Mechanics Reviews*, 54(4), pp. 331-390.

[10] Rozvany, G., 2001, "Aims, scope, methods, history and unified terminology of computer-aided topology optimization in structural mechanics," *Structural and Multidisciplinary Optimization*, 21(2), pp. 90-108.

[11] Suzuki, K., and Kikuchi, N., 1991, "A homogenization method for shape and topology optimization," *Computer methods in applied mechanics and engineering*, 93(3), pp. 291-318.

[12] Rosen, D., 2014, "Design for additive manufacturing: Past, present, and future directions," *Journal of Mechanical Design*, 136(9), p. 090301.

[13] Doubrovski, Z., Verlinden, J. C., and Geraedts, J. M., "Optimal design for additive manufacturing: opportunities and

challenges," Proc. ASME 2011 International Design Engineering Technical Conferences and Computers and Information in Engineering Conference, American Society of Mechanical Engineers, pp. 635-646.

[14] Zegard, T., and Paulino, G. H., 2016, "Bridging topology optimization and additive manufacturing," *Structural and Multidisciplinary Optimization*, 53(1), pp. 175-192.

[15] Gaynor, A. T., Meisel, N. A., Williams, C. B., and Guest, J. K., 2014, "Topology optimization for additive manufacturing: considering maximum overhang constraint," Proc. 15th AIAA/ISSMO multidisciplinary analysis and optimization conference, p. 2036.

[16] Dede, E. M., Joshi, S. N., and Zhou, F., 2015, "Topology optimization, additive layer manufacturing, and experimental testing of an air-cooled heat sink," *Journal of Mechanical Design*, 137(11), p. 111403.

[17] Baumers, M., Tuck, C., Wildman, R., Ashcroft, I., Rosamond, E., and Hague, R., 2012, "Combined Build-Time, Energy Consumption and Cost Estimation for Direct Metal Laser Sintering," Proc. From Proceedings of Twenty Third Annual International Solid Freeform Fabrication Symposium—An Additive Manufacturing Conference.

[18] Francois, M. M., Sun, A., King, W. E., Henson, N. J., Turret, D., Bronkhorst, C. A., Carlson, N. N., Newman, C. K., Haut, T., and Bakosi, J., 2017, "Modeling of additive manufacturing processes for metals: Challenges and opportunities," *Current Opinion in Solid State and Materials Science*.

[19] Brackett, D., Ashcroft, I., and Hague, R., 2011, "Topology optimization for additive manufacturing," Proc. Proceedings of the solid freeform fabrication symposium, Austin, TX, pp. 348-362.

[20] Arisoy, Y. M., Criales, L. E., Özel, T., Lane, B., Moylan, S., and Donmez, A., 2016, "Influence of scan strategy and process parameters on microstructure and its optimization in additively manufactured nickel alloy 625 via laser powder bed fusion," *Int J Adv Manuf Technol*, pp. 1-25.

[21] Aboutaleb, A. M., Bian, L., Elwany, A., Shamsaei, N., Thompson, S. M., and Tapia, G., 2017, "Accelerated process optimization for laser-based additive manufacturing by leveraging similar prior studies," *IISE Transactions*, 49(1), pp. 31-44.

[22] Martukanitz, R., Michaleris, P., Palmer, T., DeRoy, T., Liu, Z.-K., Otis, R., Heo, T. W., and Chen, L.-Q., 2014, "Toward an integrated computational system for describing the additive manufacturing process for metallic materials," *Additive Manufacturing*, 1, pp. 52-63.

[23] Højbjerg, K., 2011, "Additive manufacturing of porous metal components," Proc. 6th International Conference on Additive Manufacturing, Loughborough.

[24] Mahshid, R., Hansen, H. N., and Højbjerg, K. L., 2016, "Strength analysis and modeling of cellular lattice structures manufactured using selective laser melting for tooling applications," *Materials & Design*, 104, pp. 276-283.

[25] Ponche, R., Hascoët, J.-Y., Kerbrat, O., and Mognol, P., 2012, "A new global approach to design for additive

manufacturing: A method to obtain a design that meets specifications while optimizing a given additive manufacturing process is presented in this paper," *Virtual and Physical Prototyping*, 7(2), pp. 93-105.

[26] Bendsøe, M. P., and Kikuchi, N., 1988, "Generating optimal topologies in structural design using a homogenization method," *Computer methods in applied mechanics and engineering*, 71(2), pp. 197-224.

[27] Gardan, N., and Schneider, A., 2015, "Topological optimization of internal patterns and support in additive manufacturing," *Journal of Manufacturing Systems*, 37, pp. 417-425.

[28] Chu, C., Graf, G., and Rosen, D. W., 2008, "Design for additive manufacturing of cellular structures," *Computer-Aided Design and Applications*, 5(5), pp. 686-696.

[29] Bendsøe, M. P., 1989, "Optimal shape design as a material distribution problem," *Structural optimization*, 1(4), pp. 193-202.

[30] Rozvany, G. I., Zhou, M., and Birker, T., 1992, "Generalized shape optimization without homogenization," *Structural optimization*, 4(3-4), pp. 250-252.

[31] Ulu, E., Korkmaz, E., Yay, K., Ozdoganlar, O. B., and Kara, L. B., 2015, "Enhancing the structural performance of additively manufactured objects through build orientation optimization," *Journal of Mechanical Design*, 137(11), p. 111410.

[32] Hopkinson, N., and Dicknes, P., 2003, "Analysis of rapid manufacturing—using layer manufacturing processes for production," *Proceedings of the Institution of Mechanical Engineers, Part C: Journal of Mechanical Engineering Science*, 217(1), pp. 31-39.

[33] Ruffo, M., Tuck, C., and Hague, R., 2006, "Cost estimation for rapid manufacturing-laser sintering production for low to medium volumes," *Proceedings of the Institution of Mechanical Engineers, Part B: Journal of Engineering Manufacture*, 220(9), pp. 1417-1427.

[34] Lindemann, C., Jahnke, U., Moi, M., and Koch, R., 2012, "Analyzing product lifecycle costs for a better understanding of cost drivers in additive manufacturing," Proc. 23th Annual International Solid Freeform Fabrication Symposium—An Additive Manufacturing Conference. Austin Texas USA 6th-8th August.

[35] Lindemann, C., Jahnke, U., Moi, M., and Koch, R., 2013, "Impact and Influence Factors of Additive Manufacturing on Product Lifecycle Costs," Proc. Proc. of the Solid Freeform Fabrication Symposium, pp. 998-1009.

[36] Baumers, M., Dickens, P., Tuck, C., and Hague, R., 2015, "The cost of additive manufacturing: machine productivity, economies of scale and technology-push," *Technological Forecasting and Social Change*.

[37] Rickenbacher, L., Spierings, A., and Wegener, K., 2013, "An integrated cost-model for selective laser melting (SLM)," *Rapid Prototyping Journal*, 19(3), pp. 208-214.

[38] Yim, S., and Rosen, D., 2012, "Build Time and Cost Models for Additive Manufacturing Process Selection," (45011), pp. 375-382.

- [39] Yao, X., Moon, S. K., and Bi, G., 2016, "A cost-driven design methodology for additive manufactured variable platforms in product families," *Journal of Mechanical Design*, 138(4), p. 041701.
- [40] Busch, J. V., and Field III, F. R., 1988, "Technical cost modeling," *Blow Molding Handbook*, pp. 839-871.
- [41] Fuchs, E. R., Field, F. R., Roth, R., and Kirchain, R. E., 2008, "Strategic materials selection in the automobile body: Economic opportunities for polymer composite design," *Composites science and technology*, 68(9), pp. 1989-2002.
- [42] Marallo, S. L., and Dieffenbach, J., 1994, "Manufacturing cost analysis for electronic packaging," *Proc. Economics of Design, Test, and Manufacturing, 1994. Proceedings., Third International Conference on the, IEEE*, p. 90.
- [43] Fuchs, E. R., Bruce, E., Ram, R., and Kirchain, R. E., 2006, "Process-based cost modeling of photonics manufacture: the cost competitiveness of monolithic integration of a 1550-nm DFB laser and an electroabsorptive modulator on an InP platform," *Journal of lightwave technology*, 24(8), p. 3175.
- [44] Laureijs, R. E., Roca, J. B., Narra, S. P., Montgomery, C., Beuth, J. L., and Fuchs, E. R., 2016, "Metal Additive Manufacturing: Cost Competitive Beyond Low Volumes," *Journal of Manufacturing Science and Engineering*.
- [45] Gockel, J., Beuth, J., and Taminger, K., 2014, "Integrated control of solidification microstructure and melt pool dimensions in electron beam wire feed additive manufacturing of Ti-6Al-4V," *Additive Manufacturing*, 1, pp. 119-126.
- [46] Cunningham, R., Narra, S. P., Ozturk, T., Beuth, J., and Rollett, A., 2016, "Evaluating the effect of processing parameters on porosity in electron beam melted Ti-6Al-4V via synchrotron X-ray microtomography," *JOM*, 68(3), pp. 765-771.
- [47] Seifi, M., Christiansen, D., Beuth, J., Harrysson, O., and Lewandowski, J. J., 2016, "Process mapping, fracture and fatigue behavior of Ti-6Al-4V produced by EBM additive manufacturing," *Proc. Proceedings of World Conference on Titanium, 13th, TMS/Wiley Warrendale, PA/Hoboken, NJ*, pp. 1373-1377.
- [48] Lewandowski, J. J., and Seifi, M., 2016, "Metal Additive Manufacturing: A Review of Mechanical Properties," *Annual Review of Materials Research*, 46(1).
- [49] Gockel, J., and Beuth, J., 2013, "Understanding Ti-6Al-4V microstructure control in additive manufacturing via process maps," *Solid Freeform Fabrication Proceedings, Austin, TX, Aug*, pp. 12-14.
- [50] Beuth, J., Fox, J., Gockel, J., Montgomery, C., Yang, R., Qiao, H., Soylemez, E., Reeseewatt, P., Anvari, A., and Narra, S., 2013, "Process mapping for qualification across multiple direct metal additive manufacturing processes," *Proc. Proceedings of SFF Symposium., Austin, TX, Aug*, pp. 12-14.
- [51] Beuth, J., and Klingbeil, N., 2001, "The role of process variables in laser-based direct metal solid freeform fabrication," *JOM Journal of the Minerals, Metals and Materials Society*, 53(9), pp. 36-39.
- [52] Montgomery, C., Beuth, J., Sheridan, L., and Klingbeil, N., 2015, "Process mapping of Inconel 625 in laser powder bed additive manufacturing," *Proc. Solid Freeform Fabrication Symposium*, pp. 1195-1204.
- [53] Xu, W., Brandt, M., Sun, S., Elambasseril, J., Liu, Q., Latham, K., Xia, K., and Qian, M., 2015, "Additive manufacturing of strong and ductile Ti-6Al-4V by selective laser melting via in situ martensite decomposition," *Acta Materialia*, 85, pp. 74-84.
- [54] Sergueeva, A., Stolyarov, V., Valiev, R., and Mukherjee, A., 2001, "Advanced mechanical properties of pure titanium with ultrafine grained structure," *Scripta Materialia*, 45(7), pp. 747-752.
- [55] Leuders, S., Vollmer, M., Brenne, F., Tröster, T., and Niendorf, T., 2015, "Fatigue strength prediction for titanium alloy TiAl6V4 manufactured by selective laser melting," *Metallurgical and Materials Transactions A*, 46(9), pp. 3816-3823.
- [56] Callister, W. D., and Rethwisch, D. G., 2011, *Materials science and engineering*, John Wiley & Sons NY.
- [57] Tang, M., and Pistorius, P. C., 2017, "Anisotropic Mechanical Behavior of AlSi10Mg Parts Produced by Selective Laser Melting," *JOM*, pp. 1-7.
- [58] Rosenthal, D., 1941, "Mathematical theory of heat distribution during welding and cutting," *Welding journal*, 20(5), pp. 220s-234s.
- [59] Bonnetier, E., and Jouve, F., 1998, "Checkerboard instabilities in topological shape optimization algorithms," *Proc. Proceedings of the Conference on Inverse Problems, Control and Shape Optimization PICO*.
- [60] Sigmund, O., 2001, "A 99 line topology optimization code written in Matlab," *Structural and multidisciplinary optimization*, 21(2), pp. 120-127.
- [61] Liu, K., and Tovar, A., 2014, "An efficient 3D topology optimization code written in Matlab," *Structural and Multidisciplinary Optimization*, 50(6), pp. 1175-1196.
- [62] Atzeni, E., and Salmi, A., 2012, "Economics of additive manufacturing for end-usable metal parts," *Int J Adv Manuf Technol*, 62(9-12), pp. 1147-1155.
- [63] Allen, J., 2006, "An investigation into the comparative costs of additive manufacture vs. machine from solid for aero engine parts," DTIC Document.

ANNEX A

DERIVATIONS OF COST AND OPTIMIZATION EQUATIONS

The production costs can be broken into material based costs and time-based costs. The material-based costs include the material required for printing the design of the part and material scrap that is lost during powder recovery and recycling. The time-based cost includes the machine cost allocated to the production time, the energy cost and other costs depending on the production time such as labor. The production costs can be written as

$$C = C_{mat} + C_{time}$$

$$= C_{mat,part} + C_{mat,waste} + C_{time,machine} + C_{time,labor} + C_{time,energy}$$

where $C_{mat,part}$ is the material cost of the part, $C_{mat,waste}$ is the cost of the waste material, $C_{time,machine}$ is the amortized cost of the AM machine, $C_{time,labor}$ is the cost of labor, and $C_{time,energy}$ is the cost of energy.

$$C_{mat,part} = c_m \rho V_{part}$$

$$C_{mat,waste} = c_m \rho \eta (V_{envelope} - V_{part})$$

$$C_{time,machine} = c_{mach} t = \frac{c_{invest} + c_{maintain} * L}{L * H} t$$

$$C_{time,labor} = c_{labor} t$$

$$C_{time,energy} = \int_{t_0}^t c_{elec} (P + P_0) dt$$

where c is the unit price or cost of different segment, ρ is the material density, V is the volume of part or machine build envelope, t is production time for the part, L is machine life time, H is the machine annual operation time, P is the power required for printing and P_0 is the stand-by power required for MAM machines. The cost formulation can be further reduced to:

$$C = c_m \rho V_{part} + c_m \rho \eta (V_{envelope} - V_{part}) + \frac{c_{invest} + c_{maintain} * L}{L * H} t + c_{labor} t + \int_{t_0}^t c_{elec} (P + P_0) dt$$

$$= c_m \rho (1 - \eta) V_{part} + \left(\frac{c_{invest} + c_{maintain} * L}{L * H} + c_{labor} \right) t + c_{elec} \int_{t_0}^t P dt + c_m \rho \eta V_{envelope} + c_{elec} P_0 t$$

$$= A_1 V_{part} + A_2 t + A_3 \int_{t_0}^t P dt + A_4$$

The Rosenthal equation is as follows:

$$\dot{T} = 2\pi k (T_{solidus} - T_0) (T_{liquidus} - T_0) \frac{v}{\alpha P}$$

where \dot{T} is the cooling rate, $T_{solidus}$ and $T_{liquidus}$ are the liquidus and solidus temperatures, and T_0 is the plate temperature.

The maximum compliance of the structure is derived by

$$c_o(\tilde{x}_i) = E_i(\tilde{x}_i) \mathbf{u}_i^T \mathbf{k}_0 \mathbf{u}_i = E_i(\tilde{x}_i) \mathbf{u}_i^T (\mathbf{B}_i^T \mathbf{C}_o \mathbf{B}_i) \mathbf{u}_i$$

$$= E_i(\tilde{x}_i) (\mathbf{u}_i^T \mathbf{B}_i^T) \mathbf{C}_o (\mathbf{B}_i \mathbf{u}_i)$$

$$= E_i(\tilde{x}_i) (\mathbf{C}_0^{-1} \boldsymbol{\sigma}_i)^T \mathbf{C}_o (\mathbf{C}_0^{-1} \boldsymbol{\sigma}_i)$$

$$= E_i(\tilde{x}_i) \boldsymbol{\sigma}_i^T (\mathbf{C}_0^{-1})^T \boldsymbol{\sigma}_i$$

$$\leq E_i(\tilde{x}_i) k \mathbf{Y}_i^T (\mathbf{C}_0^{-1})^T k \mathbf{Y}_i$$

$$= E_i(\tilde{x}_i) k^2 \mathbf{Y}_i^T (\tilde{\mathbf{x}}, \tilde{\mathbf{P}}, \tilde{\mathbf{v}}) (\mathbf{C}_0^{-1})^T \mathbf{Y}_i(\tilde{\mathbf{x}}, \tilde{\mathbf{P}}, \tilde{\mathbf{v}})$$

with

$$Y_i = Y_i(x_i, P_i, v_i) = Y_{min} + x_i^p (\sigma_y - Y_{min})$$

$$= Y_{min} + x_i^p \left\{ a_3 \left[\frac{2(a_1 \alpha P_i + a_2)}{\pi v_i} \right]^{\frac{1}{4}} + a_4 - Y_{min} \right\}$$

and k is the safety factor.